Measurement of singly Cabibbo-suppressed decays $D \to \omega\pi\pi$

M. Ablikim,[1] M. N. Achasov,[10,c] P. Adlarson,[64] S. Ahmed,[15] M. Albrecht,[4] A. Amoroso,[63a,63c] Q. An,[60,48] Anita,[21] Y. Bai,[47] O. Bakina,[29] R. Baldini Ferroli,[23a] I. Balossino,[24a] Y. Ban,[38,k] K. Begzsuren,[26] J. V. Bennett,[5] N. Berger,[28] M. Bertani,[23a] D. Bettoni,[24a] F. Bianchi,[63a,63c] J. Biernat,[64] J. Bloms,[57] A. Bortone,[63a,63c] I. Boyko,[29] R. A. Briere,[5] H. Cai,[65] X. Cai,[1,48] A. Calcaterra,[23a] G. F. Cao,[1,52] N. Cao,[1,52] S. A. Cetin,[51b] J. F. Chang,[1,48] W. L. Chang,[1,52] G. Chelkov,[29,b] D. Y. Chen,[6] G. Chen,[1] H. S. Chen,[1,52] M. L. Chen,[1,48] S. J. Chen,[36] X. R. Chen,[25] Y. B. Chen,[1,48] W. S. Cheng,[63c] G. Cibinetto,[24a] F. Cossio,[63c] X. F. Cui,[37] H. L. Dai,[1,48] J. P. Dai,[42,g] X. C. Dai,[1,52] A. Dbeyssi,[15] R. B. de Boer,[4] D. Dedovich,[29] Z. Y. Deng,[1] A. Denig,[28] I. Denysenko,[29] M. Destefanis,[63a,63c] F. De Mori,[63a,63c] Y. Ding,[34] C. Dong,[37] J. Dong,[1,48] L. Y. Dong,[1,52] M. Y. Dong,[1,48,52] S. X. Du,[68] J. Fang,[1,48] S. S. Fang,[1,52] Y. Fang,[1] R. Farinelli,[24a] L. Fava,[63b,63c] F. Feldbauer,[4] G. Felici,[23a] C. Q. Feng,[60,48] M. Fritsch,[4] C. D. Fu,[1] Y. Fu,[1] X. L. Gao,[60,48] Y. Gao,[38,k] Y. Gao,[61] Y. G. Gao,[6] I. Garzia,[24a,24b] E. M. Gersabeck,[55] A. Gilman,[56] K. Goetzen,[11] L. Gong,[37] W. X. Gong,[1,48] W. Gradl,[28] M. Greco,[63a,63c] L. M. Gu,[36] M. H. Gu,[1,48] S. Gu,[2] Y. T. Gu,[13] C. Y. Guan,[1,52] A. Q. Guo,[22] L. B. Guo,[35] R. P. Guo,[40] Y. P. Guo,[28] Y. P. Guo,[9,h] A. Guskov,[29] S. Han,[65] T. T. Han,[41] T. Z. Han,[9,h] X. Q. Hao,[16] F. A. Harris,[53] K. L. He,[1,52] F. H. Heinsius,[4] T. Held,[4] Y. K. Heng,[1,48,52] M. Himmelreich,[11,f] T. Holtmann,[4] Y. R. Hou,[52] Z. L. Hou,[1] H. M. Hu,[1,52] J. F. Hu,[42,g] T. Hu,[1,48,52] Y. Hu,[1] G. S. Huang,[60,48] L. Q. Huang,[61] X. T. Huang,[41] Z. Huang,[38,k] N. Huesken,[57] T. Hussain,[62] W. Ikegami Andersson,[64] W. Imoehl,[22] M. Irshad,[60,48] S. Jaeger,[4] S. Janchiv,[26,j] Q. Ji,[1] Q. P. Ji,[16] X. B. Ji,[1,52] X. L. Ji,[1,48] H. B. Jiang,[41] X. S. Jiang,[1,48,52] X. Y. Jiang,[37] J. B. Jiao,[41] Z. Jiao,[18] S. Jin,[36] Y. Jin,[54] T. Johansson,[64] N. Kalantar-Nayestanaki,[31] X. S. Kang,[34] R. Kappert,[31] M. Kavatsyuk,[31] B. C. Ke,[43,1] I. K. Keshk,[4] A. Khoukaz,[57] P. Kiese,[28] R. Kiuchi,[1] R. Kliemt,[11] L. Koch,[30] O. B. Kolcu,[51b,e] B. Kopf,[4] M. Kuemmel,[4] M. Kuessner,[4] A. Kupsc,[64] M. G. Kurth,[1,52] W. Kühn,[30] J. J. Lane,[55] J. S. Lange,[30] P. Larin,[15] L. Lavezzi,[63c] H. Leithoff,[28] M. Lellmann,[28] T. Lenz,[28] C. Li,[39] C. H. Li,[33] Cheng Li,[60,48] D. M. Li,[68] F. Li,[1,48] G. Li,[1] H. B. Li,[1,52] H. J. Li,[9,h] J. L. Li,[41] J. Q. Li,[4] Ke Li,[1] L. K. Li,[1] Lei Li,[3] P. L. Li,[60,48] P. R. Li,[32] S. Y. Li,[50] W. D. Li,[1,52] W. G. Li,[1] X. H. Li,[60,48] X. L. Li,[41] Z. B. Li,[49] Z. Y. Li,[49] H. Liang,[60,48] H. Liang,[1,52] Y. F. Liang,[45] Y. T. Liang,[25] L. Z. Liao,[1,52] J. Libby,[21] C. X. Lin,[49] B. Liu,[42,g] B. J. Liu,[1] C. X. Liu,[1] D. Liu,[60,48] D. Y. Liu,[42,g] F. H. Liu,[44] Fang Liu,[1] Feng Liu,[6] H. B. Liu,[13] H. M. Liu,[1,52] Huanhuan Liu,[1] Huihui Liu,[17] J. B. Liu,[60,48] J. Y. Liu,[1,52] K. Liu,[1] K. Y. Liu,[34] Ke Liu,[6] L. Liu,[60,48] Q. Liu,[52] S. B. Liu,[60,48] Shuai Liu,[46] T. Liu,[1,52] X. Liu,[32] Y. B. Liu,[37] Z. A. Liu,[1,48,52] Z. Q. Liu,[41] Y. F. Long,[38,k] X. C. Lou,[1,48,52] F. X. Lu,[16] H. J. Lu,[18] J. D. Lu,[1,52] J. G. Lu,[1,48] X. L. Lu,[1] Y. Lu,[1] Y. P. Lu,[1,48] C. L. Luo,[35] M. X. Luo,[67] P. W. Luo,[49] T. Luo,[9,h] X. L. Luo,[1,48] S. Lusso,[63c] X. R. Lyu,[52] F. C. Ma,[34] H. L. Ma,[1] L. L. Ma,[41] M. M. Ma,[1,52] Q. M. Ma,[1] R. Q. Ma,[1,52] R. T. Ma,[52] X. N. Ma,[37] X. X. Ma,[1,52] X. Y. Ma,[1,48] Y. M. Ma,[41] F. E. Maas,[15] M. Maggiora,[63a,63c] S. Maldaner,[28] S. Malde,[58] Q. A. Malik,[62] A. Mangoni,[23b] Y. J. Mao,[38,k] Z. P. Mao,[1] S. Marcello,[63a,63c] Z. X. Meng,[54] J. G. Messchendorp,[31] G. Mezzadri,[24a] T. J. Min,[36] R. E. Mitchell,[22] X. H. Mo,[1,48,52] Y. J. Mo,[6] N. Yu. Muchnoi,[10,c] H. Muramatsu,[56] S. Nakhoul,[11,f] Y. Nefedov,[29] F. Nerling,[11,f] I. B. Nikolaev,[10,c] Z. Ning,[1,48] S. Nisar,[8,i] S. L. Olsen,[52] Q. Ouyang,[1,48,52] S. Pacetti,[23b] X. Pan,[46] Y. Pan,[55] A. Pathak,[1] P. Patteri,[23a] M. Pelizaeus,[4] H. P. Peng,[60,48] K. Peters,[11,f] J. Pettersson,[64] J. L. Ping,[35] R. G. Ping,[1,52] A. Pitka,[4] R. Poling,[56] V. Prasad,[60,48] H. Qi,[60,48] H. R. Qi,[50] M. Qi,[36] T. Y. Qi,[2] S. Qian,[1,48] W.-B. Qian,[52] Z. Qian,[49] C. F. Qiao,[52] L. Q. Qin,[12] X. P. Qin,[13] X. S. Qin,[4] Z. H. Qin,[1,48] J. F. Qiu,[1] S. Q. Qu,[37] K. H. Rashid,[62] K. Ravindran,[21] C. F. Redmer,[28] A. Rivetti,[63c] V. Rodin,[31] M. Rolo,[63c] G. Rong,[1,52] Ch. Rosner,[15] M. Rump,[57] A. Sarantsev,[29,d] Y. Schelhaas,[28] C. Schnier,[4] K. Schoenning,[64] D. C. Shan,[46] W. Shan,[19] X. Y. Shan,[60,48] M. Shao,[60,48] C. P. Shen,[2] P. X. Shen,[37] X. Y. Shen,[1,52] H. C. Shi,[60,48] R. S. Shi,[1,52] X. Shi,[1,48] X. D. Shi,[60,48] J. J. Song,[41] Q. Q. Song,[60,48] W. M. Song,[27] Y. X. Song,[38,k] S. Sosio,[63a,63c] S. Spataro,[63a,63c] F. F. Sui,[41] G. X. Sun,[1] J. F. Sun,[16] L. Sun,[65] S. S. Sun,[1,52] T. Sun,[1,52] W. Y. Sun,[35] X. Sun,[20,l] Y. J. Sun,[60,48] Y. K. Sun,[60,48] Y. Z. Sun,[1] Z. T. Sun,[1] Y. H. Tan,[65] Y. X. Tan,[60,48] C. J. Tang,[45] G. Y. Tang,[1] J. Tang,[49] V. Thoren,[64] B. Tsednee,[26] I. Uman,[51d] B. Wang,[1] B. L. Wang,[52] C. W. Wang,[36] D. Y. Wang,[38,k] H. P. Wang,[1,52] K. Wang,[1,48] L. L. Wang,[1] M. Wang,[41] M. Z. Wang,[38,k] Meng Wang,[1,52] W. H. Wang,[65] W. P. Wang,[60,48] X. Wang,[38,k] X. F. Wang,[32] X. L. Wang,[9,h] Y. Wang,[49] Y. Wang,[60,48] Y. D. Wang,[15] Y. F. Wang,[1,48,52] Y. Q. Wang,[1] Z. Wang,[1,48] Z. Y. Wang,[1] Ziyi Wang,[52] Zongyuan Wang,[1,52] D. H. Wei,[12] P. Weidenkaff,[28] F. Weidner,[57] S. P. Wen,[1] D. J. White,[55] U. Wiedner,[4] G. Wilkinson,[58] M. Wolke,[64] L. Wollenberg,[4] J. F. Wu,[1,52] L. H. Wu,[1] L. J. Wu,[1,52] X. Wu,[9,h] Z. Wu,[1,48] L. Xia,[60,48] H. Xiao,[9,h] S. Y. Xiao,[1] Y. J. Xiao,[1,52] Z. J. Xiao,[35] X. H. Xie,[38,k] Y. G. Xie,[1,48] Y. H. Xie,[6] T. Y. Xing,[1,52] X. A. Xiong,[1,52] G. F. Xu,[1] J. J. Xu,[36] Q. J. Xu,[14] W. Xu,[1,52] X. P. Xu,[46] L. Yan,[63a,63c] L. Yan,[9,h] W. B. Yan,[60,48] W. C. Yan,[68] Xu Yan,[46] H. J. Yang,[42,g] H. X. Yang,[1] L. Yang,[65] R. X. Yang,[60,48] S. L. Yang,[1,52] Y. H. Yang,[36] Y. X. Yang,[12] Yifan Yang,[1,52] Zhi Yang,[25] M. Ye,[1,48] M. H. Ye,[7] J. H. Yin,[1] Z. Y. You,[49] B. X. Yu,[1,48,52] C. X. Yu,[37] G. Yu,[1,52] J. S. Yu,[20,l] T. Yu,[61] C. Z. Yuan,[1,52] W. Yuan,[63a,63c] X. Q. Yuan,[38,k] Y. Yuan,[1] Z. Y. Yuan,[49] C. X. Yue,[33] A. Yuncu,[51b,a] A. A. Zafar,[62] Y. Zeng,[20,l] B. X. Zhang,[1] Guangyi Zhang,[16] H. H. Zhang,[49] H. Y. Zhang,[1,48] J. L. Zhang,[66] J. Q. Zhang,[4] J. W. Zhang,[1,48,52] J. Y. Zhang,[1] J. Z. Zhang,[1,52] Jianyu Zhang,[1,52] Jiawei Zhang,[1,52] L. Zhang,[1] Lei Zhang,[36] S. Zhang,[49] S. F. Zhang,[36] T. J. Zhang,[42,g] X. Y. Zhang,[41] Y. Zhang,[58]

Y. H. Zhang,[1,48] Y. T. Zhang,[60,48] Yan Zhang,[60,48] Yao Zhang,[1] Yi Zhang,[9,h] Z. H. Zhang,[6] Z. Y. Zhang,[65] G. Zhao,[1] J. Zhao,[33] J. Y. Zhao,[1,52] J. Z. Zhao,[1,48] Lei Zhao,[60,48] Ling Zhao,[1] M. G. Zhao,[37] Q. Zhao,[1] S. J. Zhao,[68] Y. B. Zhao,[1,48] Y. X. Zhao Zhao,[25] Z. G. Zhao,[60,48] A. Zhemchugov,[29,b] B. Zheng,[61] J. P. Zheng,[1,48] Y. Zheng,[38,k] Y. H. Zheng,[52] B. Zhong,[35] C. Zhong,[61] L. P. Zhou,[1,52] Q. Zhou,[1,52] X. Zhou,[65] X. K. Zhou,[52] X. R. Zhou,[60,48] A. N. Zhu,[1,52] J. Zhu,[37] K. Zhu,[1] K. J. Zhu,[1,48,52] S. H. Zhu,[59] W. J. Zhu,[37] X. L. Zhu,[50] Y. C. Zhu,[60,48] Z. A. Zhu,[1,52] B. S. Zou,[1] and J. H. Zou[1]

(BESIII Collaboration)

[1]*Institute of High Energy Physics, Beijing 100049, People's Republic of China*
[2]*Beihang University, Beijing 100191, People's Republic of China*
[3]*Beijing Institute of Petrochemical Technology, Beijing 102617, People's Republic of China*
[4]*Bochum Ruhr-University, D-44780 Bochum, Germany*
[5]*Carnegie Mellon University, Pittsburgh, Pennsylvania 15213, USA*
[6]*Central China Normal University, Wuhan 430079, People's Republic of China*
[7]*China Center of Advanced Science and Technology, Beijing 100190, People's Republic of China*
[8]*COMSATS University Islamabad, Lahore Campus, Defence Road, Off Raiwind Road, 54000 Lahore, Pakistan*
[9]*Fudan University, Shanghai 200443, People's Republic of China*
[10]*G.I. Budker Institute of Nuclear Physics SB RAS (BINP), Novosibirsk 630090, Russia*
[11]*GSI Helmholtzcentre for Heavy Ion Research GmbH, D-64291 Darmstadt, Germany*
[12]*Guangxi Normal University, Guilin 541004, People's Republic of China*
[13]*Guangxi University, Nanning 530004, People's Republic of China*
[14]*Hangzhou Normal University, Hangzhou 310036, People's Republic of China*
[15]*Helmholtz Institute Mainz, Johann-Joachim-Becher-Weg 45, D-55099 Mainz, Germany*
[16]*Henan Normal University, Xinxiang 453007, People's Republic of China*
[17]*Henan University of Science and Technology, Luoyang 471003, People's Republic of China*
[18]*Huangshan College, Huangshan 245000, People's Republic of China*
[19]*Hunan Normal University, Changsha 410081, People's Republic of China*
[20]*Hunan University, Changsha 410082, People's Republic of China*
[21]*Indian Institute of Technology Madras, Chennai 600036, India*
[22]*Indiana University, Bloomington, Indiana 47405, USA*
[23a]*INFN Laboratori Nazionali di Frascati, I-00044 Frascati, Italy*
[23b]*INFN and University of Perugia, I-06100 Perugia, Italy*
[24a]*INFN Sezione di Ferrara, I-44122 Ferrara, Italy*
[24b]*University of Ferrara, I-44122 Ferrara, Italy*
[25]*Institute of Modern Physics, Lanzhou 730000, People's Republic of China*
[26]*Institute of Physics and Technology, Peace Avenue 54B, Ulaanbaatar 13330, Mongolia*
[27]*Jilin University, Changchun 130012, People's Republic of China*
[28]*Johannes Gutenberg University of Mainz, Johann-Joachim-Becher-Weg 45, D-55099 Mainz, Germany*
[29]*Joint Institute for Nuclear Research, 141980 Dubna, Moscow region, Russia*
[30]*Justus-Liebig-Universitaet Giessen, II. Physikalisches Institut, Heinrich-Buff-Ring 16, D-35392 Giessen, Germany*
[31]*KVI-CART, University of Groningen, NL-9747 AA Groningen, Netherlands*
[32]*Lanzhou University, Lanzhou 730000, People's Republic of China*
[33]*Liaoning Normal University, Dalian 116029, People's Republic of China*
[34]*Liaoning University, Shenyang 110036, People's Republic of China*
[35]*Nanjing Normal University, Nanjing 210023, People's Republic of China*
[36]*Nanjing University, Nanjing 210093, People's Republic of China*
[37]*Nankai University, Tianjin 300071, People's Republic of China*
[38]*Peking University, Beijing 100871, People's Republic of China*
[39]*Qufu Normal University, Qufu 273165, People's Republic of China*
[40]*Shandong Normal University, Jinan 250014, People's Republic of China*
[41]*Shandong University, Jinan 250100, People's Republic of China*
[42]*Shanghai Jiao Tong University, Shanghai 200240, People's Republic of China*
[43]*Shanxi Normal University, Linfen 041004, People's Republic of China*
[44]*Shanxi University, Taiyuan 030006, People's Republic of China*
[45]*Sichuan University, Chengdu 610064, People's Republic of China*
[46]*Soochow University, Suzhou 215006, People's Republic of China*
[47]*Southeast University, Nanjing 211100, People's Republic of China*

[48]State Key Laboratory of Particle Detection and Electronics, Beijing 100049, Hefei 230026, People's Republic of China
[49]Sun Yat-Sen University, Guangzhou 510275, People's Republic of China
[50]Tsinghua University, Beijing 100084, People's Republic of China
[51a]Ankara University, 06100 Tandogan, Ankara, Turkey
[51b]Istanbul Bilgi University, 34060 Eyup, Istanbul, Turkey
[51c]Uludag University, 16059 Bursa, Turkey
[51d]Near East University, Nicosia, North Cyprus, Mersin 10, Turkey
[52]University of Chinese Academy of Sciences, Beijing 100049, People's Republic of China
[53]University of Hawaii, Honolulu, Hawaii 96822, USA
[54]University of Jinan, Jinan 250022, People's Republic of China
[55]University of Manchester, Oxford Road, Manchester M13 9PL, United Kingdom
[56]University of Minnesota, Minneapolis, Minnesota 55455, USA
[57]University of Muenster, Wilhelm-Klemm-Strasse 9, 48149 Muenster, Germany
[58]University of Oxford, Keble Road, Oxford OX13RH, United Kingdom
[59]University of Science and Technology Liaoning, Anshan 114051, People's Republic of China
[60]University of Science and Technology of China, Hefei 230026, People's Republic of China
[61]University of South China, Hengyang 421001, People's Republic of China
[62]University of the Punjab, Lahore 54590, Pakistan
[63a]University of Turin, I-10125 Turin, Italy
[63b]University of Eastern Piedmont, I-15121 Alessandria, Italy
[63c]INFN, I-10125 Turin, Italy
[64]Uppsala University, Box 516, SE-75120 Uppsala, Sweden
[65]Wuhan University, Wuhan 430072, People's Republic of China
[66]Xinyang Normal University, Xinyang 464000, People's Republic of China
[67]Zhejiang University, Hangzhou 310027, People's Republic of China
[68]Zhengzhou University, Zhengzhou 450001, People's Republic of China

(Received 6 July 2020; accepted 20 August 2020; published 9 September 2020)

Using 2.93 fb^{-1} of e^+e^- collision data taken at a center-of-mass energy of 3.773 GeV by the BESIII detector at the BEPCII, we measure the branching fractions of the singly Cabibbo-suppressed decays $D \to \omega\pi\pi$ to be $\mathcal{B}(D^0 \to \omega\pi^+\pi^-) = (1.33 \pm 0.16 \pm 0.12) \times 10^{-3}$ and $\mathcal{B}(D^+ \to \omega\pi^+\pi^0) = (3.87 \pm 0.83 \pm 0.25) \times 10^{-3}$, where the first uncertainties are statistical and the second ones systematic. The statistical significances are 12.9σ and 7.7σ, respectively. The precision of $\mathcal{B}(D^0 \to \omega\pi^+\pi^-)$ is improved by a factor of 2.1 over prior measurements, and $\mathcal{B}(D^+ \to \omega\pi^+\pi^0)$ is measured for the first time. No significant signal for $D^0 \to \omega\pi^0\pi^0$ is observed, and the upper limit on the branching fraction is $\mathcal{B}(D^0 \to \omega\pi^0\pi^0) < 1.10 \times 10^{-3}$ at the 90% confidence level. The branching fractions of $D \to \eta\pi\pi$ are also measured and consistent with existing results.

DOI: 10.1103/PhysRevD.102.052003

[a]Also at Bogazici University, 34342 Istanbul, Turkey.
[b]Also at Moscow Institute of Physics and Technology, Moscow 141700, Russia.
[c]Also at Novosibirsk State University, Novosibirsk 630090, Russia.
[d]Also at NRC "Kurchatov Institute," PNPI, Gatchina 188300, Russia.
[e]Also at Istanbul Arel University, 34295 Istanbul, Turkey.
[f]Also at Goethe University Frankfurt, 60323 Frankfurt am Main, Germany.
[g]Also at Key Laboratory for Particle Physics, Astrophysics and Cosmology, Ministry of Education; Shanghai Key Laboratory for Particle Physics and Cosmology; Institute of Nuclear and Particle Physics, Shanghai 200240, People's Republic of China.
[h]Also at Key Laboratory of Nuclear Physics and Ion-beam Application (MOE) and Institute of Modern Physics, Fudan University, Shanghai 200443, People's Republic of China.
[i]Also at Harvard University, Department of Physics, Cambridge, Massachusetts 02138, USA.
[j]Present address: Institute of Physics and Technology, Peace Avenue 54B, Ulaanbaatar 13330, Mongolia.
[k]Also at State Key Laboratory of Nuclear Physics and Technology, Peking University, Beijing 100871, People's Republic of China.
[l]Also at School of Physics and Electronics, Hunan University, Changsha 410082, People's Republic of China.

I. INTRODUCTION

The study of multibody hadronic decays of charmed mesons is important to understand the decay dynamics of both strong and weak interactions. It also provides important input to the beauty sector for the test of Standard Model (SM) predictions. For instance, the self-conjugate decay $D^0 \to \omega\pi^+\pi^-$ can be used to improve the measurement of the Cabibbo-Kobayashi-Maskawa (CKM) angle γ via $B^\pm \to D^0 K^\pm$ [1–3], and the unmeasured decay $D^+ \to \omega\pi^+\pi^0$ is a potential background in the semitauonic decay $B \to D\tau\nu_\tau$. The ratio of branching fractions (BFs) $\mathcal{R}(D)$, defined as $\mathcal{B}(B \to D\tau\nu_\tau)/\mathcal{B}(B \to Dl\nu_l)(l = e, \mu)$, probes lepton flavor universality (LFU). The current world average measurement of $\mathcal{R}(D)$ is around 3.1σ away from the SM prediction [4,5], which is evidence of LFU violation. However, the BFs of many multibody hadronic decays, especially for singly Cabibbo-suppressed (SCS) or doubly Cabibbo-suppressed (DCS) decays of D mesons, are still either unknown or imprecise due to low decay rates or huge backgrounds. Precise measurements of these decays are desirable in several areas.

Until now, for the SCS decays $D \to \omega\pi\pi$, only the branching fraction of $D^0 \to \omega\pi^+\pi^-$ has been measured; CLEO found $B(D^0 \to \omega\pi^+\pi^-) = (1.6 \pm 0.5) \times 10^{-3}$ [6], where the precision is limited by low statistics. The data used in this analysis are a $\psi(3770)$ sample with an integrated luminosity of 2.93 fb^{-1} [7] collected at a center-of-mass energy of 3.773 GeV with the BESIII detector at the BEPCII collider. It provides an excellent opportunity to improve these measurements. Furthermore, in the decay $\psi(3770) \to D^0\overline{D^0}$, the D^0 and $\bar{D}^0$ mesons are coherent and of opposite CP eigenvalues. Thus, a sufficiently large sample can also be used to measure the fractional CP content of the decay $D^0 \to \omega\pi^+\pi^-$, which is necessary to relate the CP-violating observables to the CKM angle γ via the so-called quasi Gronau-London-Wyler (GLW) method [1].

In this paper, we present measurements of the absolute BFs of the SCS decays $D \to \omega\pi\pi$ with the "double tag" (DT) technique pioneered by the MARK-III Collaboration [8]. The advantage of this technique is to reduce the combinatorial backgrounds from non-$D\bar{D}$ decays with a cost of loss of the statistics. The ω mesons are reconstructed in the $\pi^+\pi^-\pi^0$ final states. We also measure the BFs for $D \to \eta\pi\pi$ with the subsequent decay $\eta \to \pi^+\pi^-\pi^0$, which are used to verify the results measured with the $\eta \to \gamma\gamma$ decay mode and theoretical models [9,10]. Throughout the paper, the charge conjugate modes are always implied, unless explicitly stated.

II. BESIII DETECTOR AND MONTE CARLO SIMULATION

BESIII is a cylindrical spectrometer covering 93% of the total solid angle. It consists of a helium-gas-based main drift chamber (MDC), a plastic scintillator time-of-flight (TOF) system, a CsI(Tl) electromagnetic calorimeter (EMC), a superconducting solenoid providing a 1.0 T magnetic field, and a muon counter. The momentum resolution of a charged particle in the MDC is 0.5% at a transverse momentum of 1 GeV/c, and the energy resolution of a photon in the EMC is 2.5(5.0)% at 1 GeV in the barrel (end-cap) region. Particle identification (PID) is performed by combining the ionization energy loss (dE/dx) measured by the MDC and the information from TOF. The details about the design and detector performance are provided in Ref. [11].

Monte Carlo (MC) simulation based on GEANT4 [12] is used to optimize the event selection criteria, study the potential backgrounds, and evaluate the detection efficiencies. The generator KKMC [13] simulates the e^+e^- collision incorporating the effects of beam energy spread and initial-state radiation (ISR). An inclusive MC sample containing $D\bar{D}$ and non-$D\bar{D}$ events, ISR production of $\psi(3686)$ and J/ψ, and continuum processes $e^+e^- \to q\bar{q}$ ($q = u, d, s$), is used to study the potential backgrounds. The known decays as specified in the Particle Data Group (PDG) [14] are simulated by EvtGen [15], while the remaining unknown decays by Lundcharm [16].

III. ANALYSIS STRATEGY

We first select "single tag" (ST) events in which the D meson candidate is reconstructed in a specific hadronic decay mode. Then the D meson candidate of interest is reconstructed with the remaining tracks. The absolute BFs for DT D decays are calculated by

$$\mathcal{B}^{\rm sig} = \frac{N^{\rm sig}_{\rm DT}}{\mathcal{B}^{\rm int}\sum_i N^i_{\rm ST}\epsilon^{{\rm sig},i}_{\rm DT}/\epsilon^i_{\rm ST}}, \quad (1)$$

where $N^{\rm sig}_{\rm DT}$ the yields of DT signal events an and $N^i_{\rm ST}$ ared ST events, $\epsilon^i_{\rm ST}$ and $\epsilon^{{\rm sig},i}_{\rm DT}$ are the ST and DT detection efficiencies for a specific ST mode i, respectively, and $\mathcal{B}^{\rm int}$ is the product of the BFs of the intermediate states ω/η and π^0 in the subsequent decays of the D meson.

IV. DATA ANALYSIS

For each tag mode, the D meson candidates are reconstructed from all possible combinations of final state particles with the following selection criteria. Charged tracks, not utilized for K^0_S reconstruction, are required to have their distance of closest approach to the interaction point (IP) be within 1 cm in the plane perpendicular to the beam and ± 10 cm along the beam. The polar angle θ with respect to the z-axis is required to satisfy $|\cos\theta| < 0.93$. PID is performed to determine likelihood $\mathcal{L}$ values for the $\pi^\pm$ and $K^\pm$ hypotheses, and $\mathcal{L}_\pi > \mathcal{L}_K$ and $\mathcal{L}_K > \mathcal{L}_\pi$ are required for the $\pi^\pm$ and $K^\pm$ candidates, respectively.

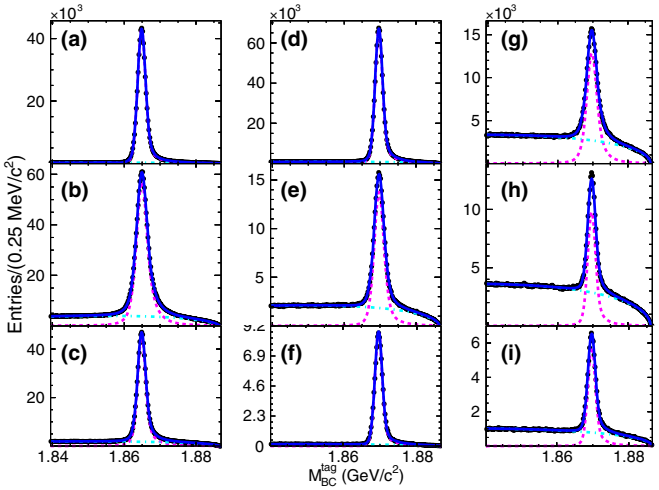

FIG. 1. Fits to the $M_{\rm BC}^{\rm tag}$ distributions for the ST modes: (a) $\bar{D}^0 \to K^+\pi^-$, (b) $\bar{D}^0 \to K^+\pi^-\pi^0$, (c) $\bar{D}^0 \to K^+\pi^-\pi^-\pi^+$, (d) $D^- \to K^+\pi^-\pi^-$, (e) $D^- \to K^+\pi^-\pi^-\pi^0$, (f) $D^- \to K_S^0\pi^-$, (g) $D^- \to K_S^0\pi^-\pi^0$, (h) $D^- \to K_S^0\pi^-\pi^-\pi^+$, and (i) $D^- \to K^+K^-\pi^-$. Black dots with error bars represent data, green dashed-dot curves are the combinatorial background, red dashed curves are the signal shape, and the blue solid curves are the total fit curves.

The K_S^0 candidates are reconstructed from a pair of oppositely charged tracks. These two tracks are assumed to be pions without performing PID and are required to be within ± 20 cm from the IP along the beam direction, but with no constraint in the transverse plane. A fit of the two pions to a common vertex is performed, and a K_S^0 candidate is required to have a χ^2 of the vertex-constrained fit less than 100. The $\pi^+\pi^-$ invariant mass $M_{\pi^+\pi^-}$ is required to be within 3 standard deviations from the K_S^0 nominal mass [14], $0.487 < M_{\pi^+\pi^-} < 0.511$ GeV/c^2. The decay length of each selected K_S^0 candidate should be further than 2 standard deviations from the IP.

Photon candidates are reconstructed from clusters of energy deposits in the EMC. The energy deposited in a nearby TOF counter is included to improve the reconstruction efficiency and energy resolution. The energy of each photon is required to be larger than 25 MeV in the barrel region ($|\cos\theta| < 0.8$) or 50 MeV in the end-cap region ($0.86 < |\cos\theta| < 0.92$). The EMC timing of the photon is required to be within 700 ns relative to the event start time to suppress electronic noise and energy deposits unrelated to the event. A π^0 candidate is reconstructed from a photon pair with an invariant mass within $[0.115, 0.150]$ GeV/c^2, and at least one photon should be detected in the EMC barrel region. To improve the momentum resolution, a kinematic fit is carried out constraining the invariant mass of the selected photon pair to the π^0 nominal mass [14], and the resultant kinematic variables are used in the subsequent analysis.

In this analysis, the ST events are selected by reconstructing $\bar{D}^0$ candidates with $K^+\pi^-$, $K^+\pi^-\pi^0$, and $K^+\pi^-\pi^-\pi^+$ final states and D^- candidates with $K^+\pi^-\pi^-$, $K^+\pi^-\pi^-\pi^0$, $K_S^0\pi^-$, $K_S^0\pi^-\pi^0$, $K_S^0\pi^-\pi^-\pi^+$, and $K^+K^-\pi^-$ final states, which comprise approximately 26% and 28% of total $\bar{D}^0$ and D^- (referred to as $\bar{D}$ later) decays, respectively. Two variables, the energy difference $\Delta E \equiv E_{\rm D} - E_{\rm beam}$ and the beam-constrained mass $M_{\rm BC}^{\rm tag} \equiv \sqrt{E_{\rm beam}^2/c^4 - p_{\rm D}^2/c^2}$, are used to identify the $\bar{D}$ candidates. Here $E_{\rm beam}$ is the beam energy, and $E_{\rm D}(p_{\rm D})$ is the reconstructed energy (momentum) of the $\bar{D}$ candidate in the e^+e^- center-of-mass system. The successful $\bar{D}$ candidate must satisfy $M_{\rm BC}^{\rm tag} > 1.84$ GeV/c^2 and a mode-dependent ΔE requirement, which is approximately 3 times its resolution. For an individual ST mode, if there are multiple candidates in an event, the one with the minimum $|\Delta E|$ is selected. In the decay process $\bar{D}^0 \to K^+\pi^-\pi^+\pi^-$, to remove backgrounds from $\bar{D}^0 \to K_S^0K^+\pi^-$, the invariant mass of any $\pi^+\pi^-$ is required to satisfy $|M_{\pi^+\pi^-} - M_{K_S^0}| > 30$ MeV/c^2, where $M_{K_S^0}$ is the nominal mass of K_S^0 [14].

To determine the ST yield, a binned maximum likelihood fit is performed to the $M_{\rm BC}^{\rm tag}$ distribution of selected candidate events for each ST mode. The signal is described by the MC simulated shape convolved with a Gaussian function which accounts for the resolution difference between data and MC simulation, and the combinatorial background is described by an ARGUS function [17] with a fixed end point parameter $E_{\rm beam}$. The fit curves are presented in Fig. 1.

The same procedure is used on the inclusive MC sample to determine the ST efficiency. The corresponding ST yields and efficiencies for each individual tag mode are summarized in Tables I and II for $\bar{D}^0$ and D^- decays, respectively. Here the yields for $\bar{D}^0 \to K^+\pi^-$, $K^+\pi^-\pi^0$, and $K^+\pi^-\pi^+\pi^-$ decays include the contributions from the DCS decays $\bar{D}^0 \to K^-\pi^+$, $K^-\pi^+\pi^0$, and $K^-\pi^+\pi^-\pi^+$, respectively.

TABLE I. The ST yields in data ($N_{\rm ST}$), the efficiencies for ST ($\varepsilon_{\rm ST}$ in %), and DT ($\varepsilon_{\rm DT}^{\rm modes}$ in %) for $\bar{D}^0$ decays. The uncertainties are statistical only.

Mode	$N_{\rm ST}^i$	$\varepsilon_{\rm ST}^i$	$\varepsilon_{\rm DT}^{\omega\pi^+\pi^-}$	$\varepsilon_{\rm DT}^{\eta\pi^+\pi^-}$	$\varepsilon_{\rm DT}^{\omega\pi^0\pi^0}$	$\varepsilon_{\rm DT}^{\eta\pi^0\pi^0}$
$K^+\pi^-$	542900 ± 780	66.7 ± 0.02	11.18 ± 0.08	12.94 ± 0.07	0.58 ± 0.02	0.56 ± 0.02
$K^+\pi^-\pi^0$	1065800 ± 1280	35.1 ± 0.01	5.92 ± 0.06	6.73 ± 0.02	0.31 ± 0.01	0.25 ± 0.01
$K^+\pi^-\pi^-\pi^+$	606310 ± 890	33.5 ± 0.01	4.48 ± 0.06	5.08 ± 0.04	0.22 ± 0.01	0.23 ± 0.01

TABLE II. The ST yields in data ($N_{\rm ST}$), the efficiencies for ST ($\varepsilon_{\rm ST}$ in %), and DT ($\varepsilon_{\rm DT}^{\rm modes}$ in %) for D^- decays. The uncertainties are statistical only.

Mode	$N_{\rm ST}^i$	$\varepsilon_{\rm ST}^i$	$\varepsilon_{\rm DT}^{\omega\pi^+\pi^0}$	$\varepsilon_{\rm DT}^{\eta\pi^+\pi^0}$
$K^+\pi^-\pi^-$	794890 ± 959	49.7 ± 0.03	2.47 ± 0.06	2.57 ± 0.02
$K^+\pi^-\pi^-\pi^0$	216720 ± 609	22.4 ± 0.03	0.56 ± 0.04	0.99 ± 0.03
$K_S^0\pi^-$	97769 ± 333	52.8 ± 0.10	2.30 ± 0.06	2.67 ± 0.03
$K_S^0\pi^-\pi^0$	224880 ± 661	27.6 ± 0.04	1.28 ± 0.04	1.29 ± 0.04
$K_S^0\pi^-\pi^-\pi^+$	130300 ± 513	36.0 ± 0.07	1.50 ± 0.04	1.56 ± 0.04
$K^-K^+\pi^-$	70299 ± 326	40.7 ± 0.11	2.39 ± 0.06	2.35 ± 0.04

For the DT candidates, we further reconstruct the decays $D^0 \to \pi^+\pi^-\pi^0\pi^+\pi^-$ and $\pi^+\pi^-\pi^0\pi^0\pi^0$ as well as $D^+ \to \pi^+\pi^-\pi^0\pi^+\pi^0$ using the remaining $\pi^\pm$ and π^0 candidates. The corresponding ΔE and $M_{\rm BC}^{\rm sig}$ requirements distinguish signal candidates from combinatorial backgrounds. The ΔE distribution is required to be within 3.0 (3.5) times of its resolution for $D^0 \to \pi^+\pi^-\pi^0\pi^+\pi^-$ ($D^0 \to \pi^+\pi^-\pi^0\pi^0\pi^0$ and $D^+ \to \pi^+\pi^-\pi^0\pi^+\pi^0$) decays. For a given signal mode, if there are multiple combinations in an event, the one with the minimum $|\Delta E|$ is selected. Since the signal final states contain multiple pions, an irreducible background with the same final state is that from the Cabibbo-favored (CF) processes including $K_S^0 \to \pi\pi$, and a candidate is vetoed if the invariant mass of any $\pi\pi$ combination lies within the K_S^0 mass window, i.e., $0.475 < M_{\pi^+\pi^-} < 0.520$ or $0.448 < M_{\pi^0\pi^0} < 0.548$ GeV/c^2. Four possible $\pi^+\pi^-\pi^0$ combinations exist in the decays $D^0 \to \pi^+\pi^-\pi^0\pi^+\pi^-$ and $D^+ \to \pi^+\pi^-\pi^0\pi^+\pi^0$, while there are three $\pi^+\pi^-\pi^0$ combinations in $D^0 \to \pi^+\pi^-\pi^0\pi^0\pi^0$. Combinations with the invariant mass $M_{\pi^+\pi^-\pi^0}$ less than 0.9 GeV/c^2 are retained for further analysis. The inclusion of multiple combinations for an event avoids peaking background in the $M_{\pi^+\pi^-\pi^0}$ distribution with a cost of additional combinatorial backgrounds.

After applying the above selection criteria in both ST and DT sides including $M_{\rm BC}^{\rm sig} > 1.84$ GeV/c^2, the $M_{\pi^+\pi^-\pi^0}$ distributions are shown in Fig. 2, where the ω and η signals are clear that might originate from either $D \to \omega/\eta\pi\pi$ decays or various background processes. The two-dimensional (2D) distribution of $M_{\rm BC}^{\rm tag}$ versus $M_{\rm BC}^{\rm sig}$ is shown in Fig. 3. The signal of $\psi(3770) \to D\bar{D}$ (including the background with the same final states, but without ω/η signals) is expected to concentrate around the intersection of $M_{\rm BC}^{\rm tag} = M_{\rm BC}^{\rm sig} = M_D$, where M_D is the D nominal mass. The background events from $\psi(3770) \to D\bar{D}$ with a correctly reconstructed D meson and an incorrectly reconstructed $\bar{D}$ meson (namely BKGI) distribute along the horizontal and vertical bands with $M_{\rm BC}^{\rm tag}(M_{\rm BC}^{\rm sig}) = M_D$. The background events from the $e^+e^- \to q\bar{q}$ process (BKGII) spread along the diagonal, and do not peak in either the $M_{\rm BC}^{\rm tag}$ or $M_{\rm BC}^{\rm sig}$ distribution. A small background including both $e^+e^- \to q\bar{q}$ and $\psi(3770) \to D\bar{D}$, with neither D nor $\bar{D}$ correctly reconstructed (BKGIII), is assumed to distribute uniformly in the $M_{\rm BC}^{\rm tag}$ versus $M_{\rm BC}^{\rm sig}$ phase space (PHSP).

To determine the signal yields (including the background with same final states but without ω/η signals), a 2D unbinned maximum likelihood fit is performed to the $M_{\rm BC}^{\rm tag}$ versus $M_{\rm BC}^{\rm sig}$ distribution of candidate events within the $\omega(\eta)$ signal region, defined as $0.74(0.52) < M_{\pi^+\pi^-\pi^0} < 0.82(0.57)$ GeV/c^2. The probability density function (PDF) includes those of signal and three kinds of backgrounds described as

(i) Signal: $\mathcal{A}(M_{\rm BC}^{\rm sig}, M_{\rm BC}^{\rm tag})$,
(ii) BKGI: $\mathcal{B}(M_{\rm BC}^{\rm tag}) \times \mathcal{C}(M_{\rm BC}^{\rm sig}; E_{\rm beam}, \xi_{M_{\rm BC}^{\rm sig}}, \rho) + \mathcal{B}(M_{\rm BC}^{\rm sig}) \times \mathcal{C}(M_{\rm BC}^{\rm tag}; E_{\rm beam}, \xi_{M_{\rm BC}^{\rm tag}}, \rho)$,
(iii) BKGII: $\mathcal{C}((M_{\rm BC}^{\rm sig} + M_{\rm BC}^{\rm tag}); 2 \cdot E_{\rm beam}, \xi, \rho)(\mathcal{F} \cdot G((M_{\rm BC}^{\rm sig} - M_{\rm BC}^{\rm tag}); 0, \sigma_0)) + (1 - \mathcal{F}) \cdot G((M_{\rm BC}^{\rm sig} - M_{\rm BC}^{\rm tag}); 0, \sigma_1))$,
(iv) BKGIII: $\mathcal{C}(M_{\rm BC}^{\rm sig}; E_{\rm beam}, \xi_{M_{\rm BC}^{\rm sig}}, \rho) \times \mathcal{C}(M_{\rm BC}^{\rm tag}; E_{\rm beam}, \xi_{M_{\rm BC}^{\rm tag}}, \rho)$,

where $\mathcal{A}$ and $\mathcal{B}$ are 2D and one-dimensional (1D) signal PDFs for $M_{\rm BC}^{\rm sig/tag}$ distributions, which are described with the simulated signal shapes convolved with 2D and 1D Gaussian functions, respectively, to account for the resolution difference between data and MC simulation. $\mathcal{C}(x, E_{\rm end}, \xi, \rho)$ is an ARGUS function [17] with a fixed end point of $E_{\rm beam}$ and two free parameters of ξ and ρ. $\mathcal{F}$ is the fraction of a Gaussian function $G(x; 0, \sigma_i)$, the mean of which is zero and the width σ_i is $(M_{\rm BC}^{\rm sig} + M_{\rm BC}^{\rm tag})$ dependent: $\sigma_i = a_i(M_{\rm BC}^{\rm sig} + M_{\rm BC}^{\rm tag}) + c_i$ $(i = 0, 1)$. $\mathcal{F}$, a_i, and c_i are floated in the fit. The projection plots of $M_{\rm BC}^{\rm tag}$ and $M_{\rm BC}^{\rm sig}$ are shown in Fig. 4, and the signal yields ($N_{\rm SG}^{\omega/\eta}$) are summarized in Table III.

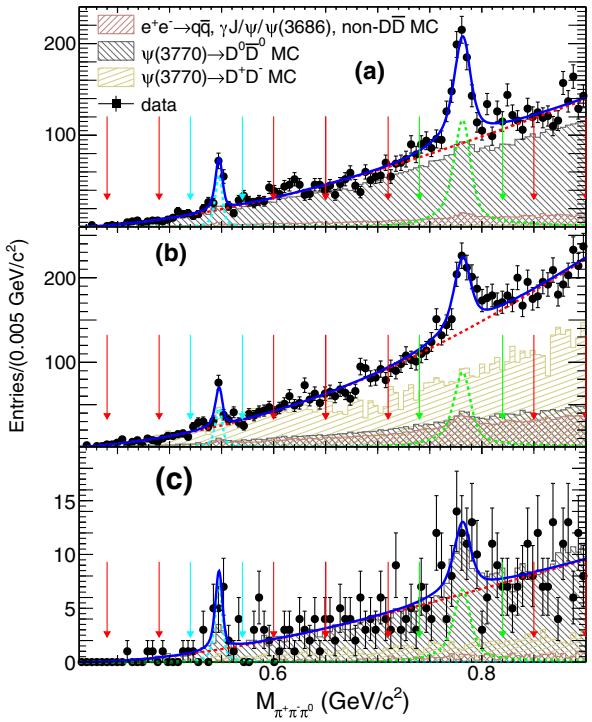

FIG. 2. Fits to the $M_{\pi^+\pi^-\pi^0}$ distributions for the processes: (a) $D^0 \to \pi^+\pi^-\pi^0\pi^+\pi^-$, (b) $D^+ \to \pi^+\pi^-\pi^0\pi^+\pi^0$, and (c) $D^0 \to \pi^+\pi^-\pi^0\pi^0\pi^0$, together with the background predictions from various MC samples shown by the histograms with diagonal pattern lines. The MC samples of $\psi(3770) \to D\bar{D}$ decays include various background processes only. Black dots with error bars are data, dashed red curves are combinatorial background, dotted cyan and green curves are η and ω signals, and the solid blue curves are the total fit curves. The two green and cyan arrow lines represent the ω and η signal regions, respectively, and the two red arrows represent their low- and high-sideband regions.

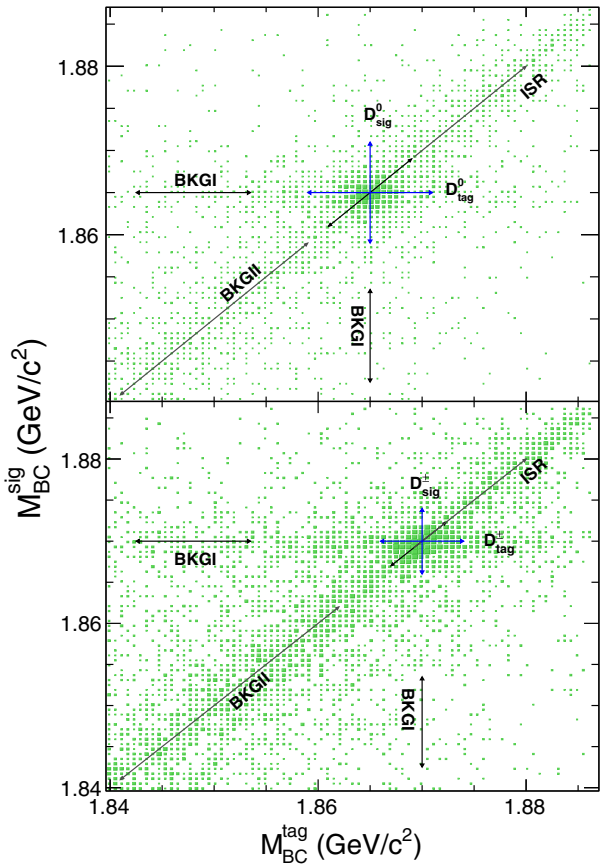

FIG. 3. The 2D distributions of $M_{\rm BC}^{\rm tag}$ versus $M_{\rm BC}^{\rm sig}$ for the DT candidate events of $\psi(3770) \to D^0\overline{D^0}$ (top) and D^+D^- (bottom).

To estimate the background with the same final states, but without ω/η signal included (BKGIV), the same fit is performed on the candidate events within the ω and η sideband regions defined as $(0.65 < M_{\pi^+\pi^-\pi^0} < 0.71) \cup (0.85 < M_{\pi^+\pi^-\pi^0} < 0.90)$ GeV/c^2 and $(0.44 < M_{\pi^+\pi^-\pi^0} < 0.49) \cup (0.60 < M_{\pi^+\pi^-\pi^0} < 0.65)$ GeV/c^2, respectively. The corresponding fit curves and signal yields ($N_{\rm SB}^{\omega/\eta}$) are shown in Fig. 5 and Table III. Additionally, there is also a small peaking background from the CF processes $D^0 \to K_S^0\omega/\eta$ (BKGV) from events surviving the K_S^0 mass window veto due to its large decay BF. The corresponding contributions ($N_{\rm peak}^{\rm BKGV}$) are estimated by

$$N_{\rm peak}^{\rm BKGV} = \mathcal{B} \cdot \sum_i \frac{N_{\rm ST}^i \varepsilon_{\rm DT}^i}{\varepsilon_{\rm ST}^i}, \tag{2}$$

where $N_{\rm ST}^i$ and $\varepsilon_{\rm ST}^i$ are the ST yield and efficiency for tag mode i, respectively, as described in Eq. (1), $\mathcal{B}$ is the product of the BFs of the decay $D^0 \to K_S^0\omega/\eta$ as well as its subsequent decays taken from the PDG [14], and $\varepsilon_{\rm DT}^i$ is the DT detection efficiency for the $D^0 \to K_S^0\omega/\eta$ decay evaluated from exclusive MC samples. The resultant $N_{\rm peak}^{\rm BKGV}$ for each individual process is summarized in Table III, where the uncertainties include those from the BFs and statistics of the MC samples.

The signal yield $N_{\rm DT}^{\rm sig}$ is given by

$$N_{\rm DT}^{\rm sig} = N_{\rm SG}^{\omega/\eta} - f \cdot N_{\rm SB}^{\omega/\eta} - N_{\rm peak}^{\rm BKGV}, \tag{3}$$

where the correction factor f is the ratio of background BKGIV yield in the ω/η signal region to that in the sideband regions. In practice, f is determined by performing a fit to the $M_{\pi^+\pi^-\pi^0}$ distribution, as shown in Fig. 2. In the fit, the ω/η signal is described by the sum of two Crystal Ball functions [18], which have the same mean and resolution values, but opposite side tails, and the background by a reversed ARGUS function defined as Eq. (4) in Ref. [19] with a fixed end point parameter corresponding to the $M_{\pi^+\pi^-\pi^0}$ threshold. The signal DT efficiencies, as summarized in Tables I and II for D^0 and D^+ decays, respectively, are determined by the same approach on the inclusive MC sample, which is the mixture of signal MC samples generated with a unified PHSP distribution and

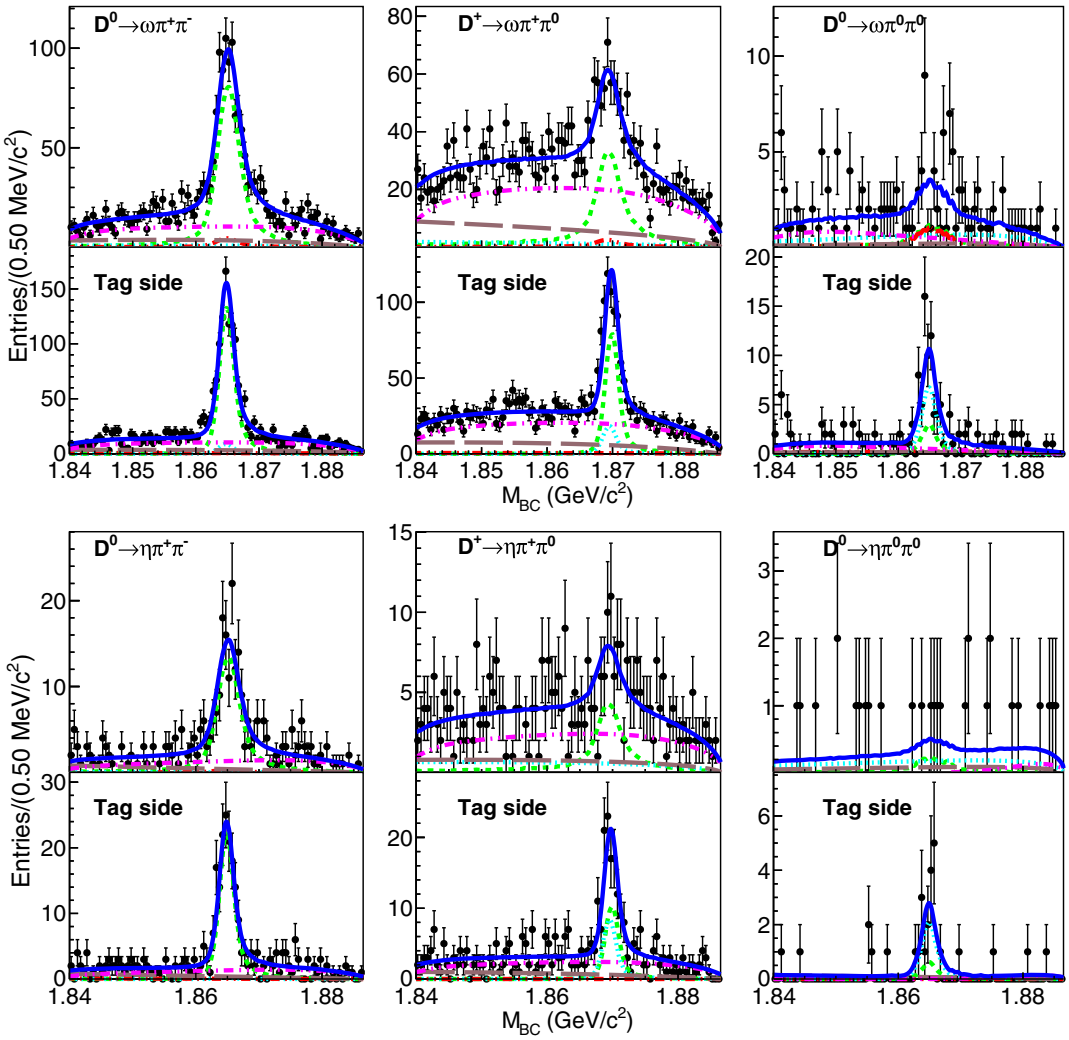

FIG. 4. Projection plots of the 2D fit to the distribution of $M_{\rm BC}^{\rm tag}$ versus $M_{\rm BC}^{\rm sig}$ for the DT candidate events in (top) ω and (bottom) η signal regions. Black dots with error bars are data, the solid blue, dashed green, dotted cyan and dashed-dotted red, long dashed-dotted pink, and long dashed brown curves represent the overall fit results, signal, BKGI, BKGII, and BKGIII, respectively. In each panel, the top plot is for $M_{\rm BC}^{\rm sig}$ and bottom for $M_{\rm BC}^{\rm tag}$.

various backgrounds. Based on the above results, the decay BFs are calculated according to Eq. (1), and are summarized in Table III. To determine the statistical significance of signals for each individual process, analogous fits are performed by fixing the signal yields to those of the sum of backgrounds BKGIV and BKGV, and the resultant likelihood values $\mathcal{L}_0$ are used to calculate the statistical significance $\mathcal{S} = \sqrt{-2\ln(\mathcal{L}_0/\mathcal{L}_{\rm max})}$, as summarized in

TABLE III. The yields of signal and individual backgrounds (see text) as well as the correction factor f, statistical significance (Sig.), $\mathcal{B}^{\rm int}$, and BFs from this measurement and the PDG [14]. Here and below, the first and second uncertainties are statistical and systematic, respectively. The upper limits are set at the 90% C.L.

Decay mode	$N_{\rm SG}^{\omega/\eta}$	$f(\%)$	$N_{\rm SB}^{\omega/\eta}$	$N_{\rm peak}^{\rm BKGV}$	$N_{\rm DT}^{\rm sig}$	Sig.	$\mathcal{B}^{\rm int}$	$\mathcal{B}^{\rm sig}(\times10^{-3})$	$\mathcal{B}_{\rm PDG}(\times10^{-3})$
$D^0\to\omega\pi^+\pi^-$	908.0 ± 39.4	74.6 ± 1.5	610.5 ± 35.1	41.4 ± 2.5	411.2 ± 48.3	12.9σ	0.882	$1.33\pm0.16\pm0.12$	1.6 ± 0.5
$D^+\to\omega\pi^+\pi^0$	474.0 ± 42.8	73.3 ± 1.2	329.0 ± 34.3	⋯	232.9 ± 49.8	7.7σ	0.872	$3.87\pm0.83\pm0.25$	⋯
$D^0\to\omega\pi^0\pi^0$	20.2 ± 10.5	75.2 ± 5.6	22.1 ± 10.0	19.0 ± 1.2	-15.4 ± 13.0	0.6σ	0.862	<1.10	⋯
$D^0\to\eta\pi^+\pi^-$	151.3 ± 14.6	42.6 ± 0.9	115.0 ± 15.3	6.1 ± 0.2	96.2 ± 16.0	8.3σ	0.227	$1.06\pm0.18\pm0.07$	1.09 ± 0.16
$D^+\to\eta\pi^+\pi^0$	61.5 ± 14.3	41.4 ± 0.7	47.3 ± 16.4	⋯	41.9 ± 15.8	3.5σ	0.224	$2.47\pm0.93\pm0.16$	1.38 ± 0.35
$D^0\to\eta\pi^0\pi^0$	5.7 ± 3.8	40.6 ± 3.3	13.1 ± 4.8	2.0 ± 0.1	-1.6 ± 4.3	0.1σ	0.221	<2.38	0.38 ± 0.13

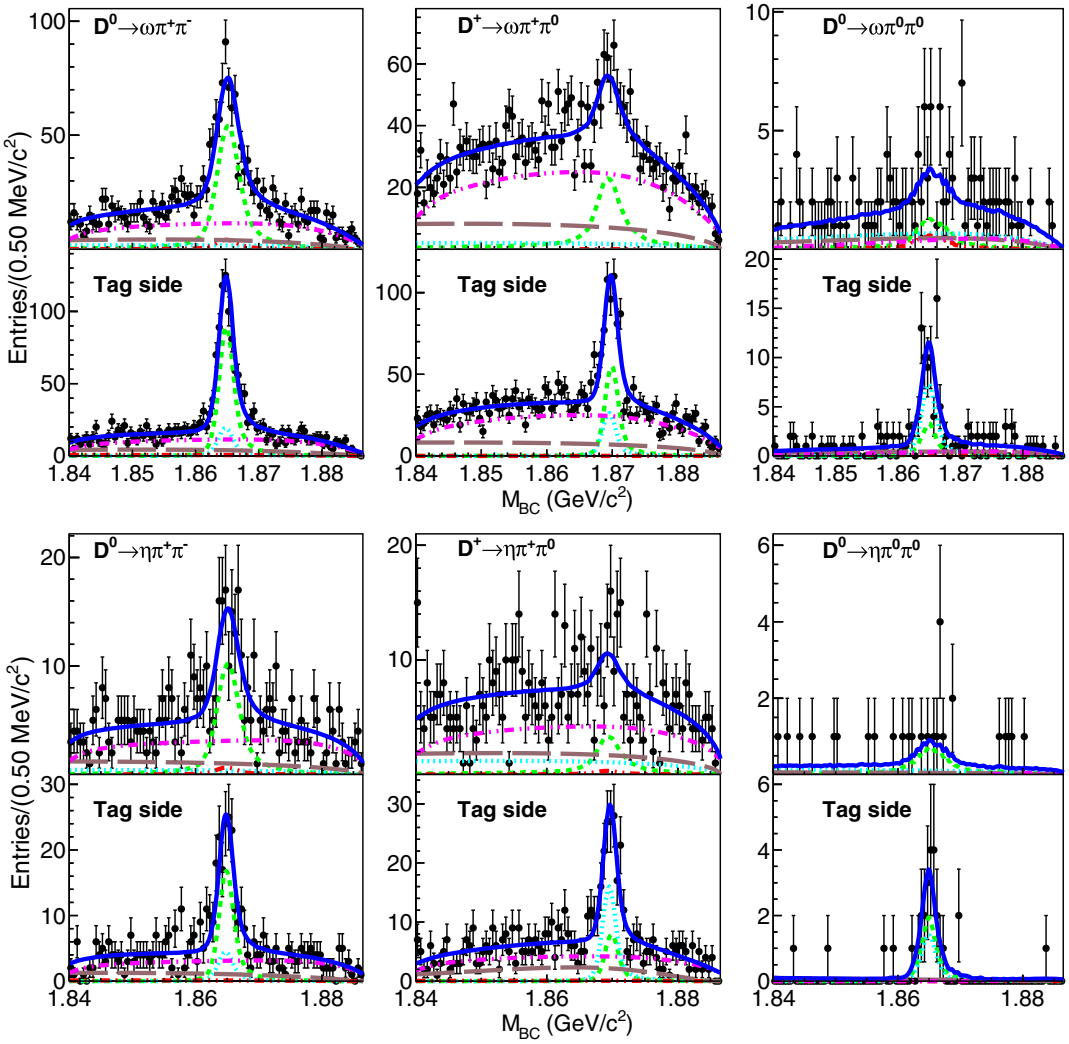

FIG. 5. Projection plots of the 2D fit to the distribution of $M_{\rm BC}^{\rm tag}$ versus $M_{\rm BC}^{\rm sig}$ for the DT candidate events in (top) ω and (bottom) η sideband regions. Black dots with error bars are data, the solid blue, dashed green, dotted cyan and dashed-dotted red, long dashed-dotted pink, and long dashed brown curves are the overall fit results, signal, BKGI, BKGII, and BKGIII, respectively. In each panel, the top plot is for $M_{\rm BC}^{\rm sig}$ and bottom for $M_{\rm BC}^{\rm tag}$.

Table III, where $\mathcal{L}_{\rm max}$ is the likelihood value of the nominal fit.

V. SYSTEMATIC UNCERTAINTIES

According to Eq. (1), the uncertainties in the BF measurements include those associated with the detection efficiencies, ST and DT event yields, as well as the BFs of the intermediate state decays.

With the DT method, the uncertainties associated with the detection efficiency from the ST side cancel. The uncertainty from the detection efficiency of the signal side includes tracking, PID, π^0 reconstruction, ΔE requirement, K_S^0 veto, and ω/η mass window requirement as well as the signal MC modeling. The uncertainties from the tracking, PID, and π^0 reconstruction are 0.5%, 0.5%, and 2.0%, respectively, which are obtained by studying a DT control sample $\psi(3770) \to D\bar{D}$ with hadronic decays of D via a partial reconstruction method [20,21]. The uncertainties associated with the ΔE requirement, K_S^0 veto, and ω/η mass window requirement are studied with control samples of $D^0 \to 2(\pi^+\pi^-)\pi^0$, $\pi^+\pi^-3\pi^0$, and $D^+ \to 2(\pi^+\pi^0)\pi^-$, which have the same final state as the signal channels, include all possible intermediate resonances, and have higher yields than the signal processes. These control samples are selected with the DT method, and their yields are obtained by fitting $M_{\rm BC}^{\rm sig}$ distributions. To study the uncertainty from ΔE, the control samples are alternatively selected with a relatively loose ΔE requirement, i.e., $|\Delta E| < 0.1$ GeV, and then with the nominal ΔE requirement. The ratio of the two signal yields is taken as the corresponding efficiency. The same approach is

implemented with both data and the inclusive MC sample, and the difference in efficiencies is taken as the uncertainty. For the K_S^0 veto uncertainty studies, we enlarge the K_S^0 veto mass window of the control samples by 10 MeV/c^2, and the relative difference in the efficiencies between data and inclusive MC sample is taken as the uncertainty. The uncertainties from the ω/η mass window requirement are studied by enlarging the corresponding mass windows by 2 MeV/c^2 and the resulting difference in efficiency between data and MC simulation is taken as the uncertainty. In the analysis, the three-body signal processes are simulated with the uniform PHSP distribution, the corresponding uncertainties are estimated with alternative MC samples, which assume $\pi\pi$ from the ρ resonance decay, and the resultant changes in efficiencies are considered as the uncertainties.

The uncertainty related to the ST yield comes from the fit procedure, and includes the signal and background shapes and the fit range. The uncertainty from the signal shape are estimated by alternatively describing the signal with a kernel estimation [22] of the signal MC derived shape convolved with a bifurcated Gaussian function. The uncertainty from the background shape is estimated by alternatively describing the shape with a modified ARGUS function [17] $(x^2/E_{\rm beam})(1-\frac{x^2}{E_{\rm beam}^2})^{\rho}\cdot e^{\xi(1-\frac{x^2}{E_{\rm beam}^2})}$. The uncertainty from the fit range of $M_{\rm BC}^{\rm tag}$ is obtained with a wider fit range, (1.835, 1.8865) GeV/c^2. The alternative fits with the above different scenarios are performed, and the resulting changes of signal yields are taken as the systematic uncertainties. The total uncertainties associated with the ST yields are the quadrature sum of individual values.

The uncertainty associated with the DT yield is from the fit procedure and background subtraction. The uncertainty from the fit procedure includes the signal and background shapes as well as the fit bias. We perform an alternative 2D fit to the $M_{\rm BC}^{\rm tag}$ versus $M_{\rm BC}^{\rm sig}$ distribution. The signal $\mathcal{A}$ ($\mathcal{B}$) is described with the kernel estimation [22] of the unbinned 2D (1D) signal MC derived shape convolved with a Gaussian function. The shape of the background is described with a modified ARGUS function [17] as described above. The relative changes in the signal yields are taken as the uncertainties. In this analysis, the 2D fit procedure is validated by repeating the fit on a large number of pseudoexperiments, which are a mixture of signals generated with various embedded events and a fixed amount of background events expected from the real data. The resultant average shift of the signal yield is taken as the systematic uncertainty. As discussed above, the background BKGIV is estimated with the events in ω/η sideband regions and incorporating a correction factor f. This induces uncertainties from the definition of sideband regions and the correction factor. The uncertainty from sideband regions is estimated by changing their ranges. The correction factor f is determined by fitting the $M_{\pi^+\pi^-\pi^0}$ distribution of surviving candidates, which is composed of the events $D\to 5\pi$ including all possible intermediate states (e.g., $\omega/\eta\to\pi^+\pi^-\pi^0$ or $\rho\to\pi\pi$) and other backgrounds that may affect f. The procedure to determine f is validated with the inclusive MC sample and its constituent $D\to 5\pi$ events in the inclusive MC sample. The resultant f values obtained with these two MC samples are found to be consistent with each other and data, and the difference between the two MC results is taken as the uncertainty. The background BKGV is estimated according to Eq. (2), and the corresponding uncertainties are from the BFs, ST yields, and detection efficiencies, where the first one has been considered as described above. Except for the uncertainty related to the K_S^0 veto requirement, which is strongly dependent on the K_S^0 mass resolution, the uncertainties associated with the other requirements and BFs are fully correlated with those of the signal, and cancel. To evaluate the uncertainty associated with the K_S^0 veto requirement, we obtain the difference of K_S^0 mass resolution between data and MC simulation using the control sample of $D^0\to K_S^0\pi^+\pi^-\pi^0$. Then we smear the $M_{\pi\pi}$ distribution of the background MC samples $D^0\to K_S^0\omega/\eta$ by a Gaussian function with the differences as parameters. The resultant change of the efficiency is taken as the uncertainty and is found to be negligible.

In this analysis, the $D^0\overline{D^0}$ pair is from the $\psi(3770)$ decays, and is quantum correlated; thus additional uncertainty associated with the strong phase is considered. In practice, the absolute BF is calculated as $\mathcal{B}_{CP\pm}^{\rm sig}=\frac{1}{1-c_f^i(2f_{CP_+}-1)}\mathcal{B}^{\rm sig}$ [23], where $\mathcal{B}^{\rm sig}$ is calculated from Eq. (1), c_f^i are the strong-phase correction factors of the flavor tags $\bar{D}^0\to K^+\pi^-, K^+\pi^-\pi^0$, and $K^+\pi^-\pi^-\pi^+$ [4,24], and f_{CP_+} is the fraction of the CP_+ component of $D^0\to\omega/\eta\pi\pi$. The f_{CP_+} value for $D^0\to\eta\pi^+\pi^-$ is taken from Ref. [25], and the corresponding systematic uncertainty is determined to be 0.8%. The uncertainties for $D^0\to\omega\pi\pi$ and $\eta\pi^0\pi^0$ are 7.3%, which are obtained by assuming $f_{CP_+}=0$ or 1 due to the limited statistics. Future BESIII $\psi(3770)$ data will enable a measurement of the f_{CP_+} of $D^0\to\omega/\eta\pi^+\pi^-$ decays [26].

The uncertainties associated with $\mathcal{B}^{\rm int}$ are obtained from Ref. [14]. All the uncertainties discussed above are summarized in Table IV. The uncertainties associated with the DT yields, which may affect the significance of observation, are classified into the additive terms, while the others are multiplicative terms. Assuming all the uncertainties to be uncorrelated, the total uncertainties in the BF measurements are obtained by adding the individual ones in quadrature. The $N_{\rm DT}^{\rm sig}$ systematic uncertainty is given by $\sqrt{{\sigma_{\rm add}}^2+(\sigma_{\rm mult}\times N_{\rm DT}^{\rm sig})^2}$, where $\sigma_{\rm add}$ and $\sigma_{\rm mult}$ are the total additive and multiplicative uncertainties, respectively.

TABLE IV. Systematic uncertainties and their sources. Here "Negl." means "Negligible."

	$D^0 \to \omega/\eta\pi^+\pi^-$		$D^0 \to \omega/\eta\pi^0\pi^0$		$D^+ \to \omega/\eta\pi^+\pi^0$	
Source	$\omega\pi^+\pi^-$	$\eta\pi^+\pi^-$	$\omega\pi^0\pi^0$	$\eta\pi^0\pi^0$	$\omega\pi^+\pi^0$	$\eta\pi^+\pi^0$
Additive systematic uncertainties (events)						
Signal PDFs	8.0	1.0	4.3	0.2	3.7	0.2
Fit bias	2.7	1.2	0.3	0.2	2.4	0.7
Nonpeaking background PDF	0.2	0.2	0.1	0.1	0.2	0.3
BKGIV contribution	3.9	4.0	3.2	0.7	4.9	0.5
BKGV contribution	Negl.	Negl.	Negl.	Negl.	$(\cdots)$	$\cdots$
Total	9.3	4.3	5.4	0.8	6.6	0.9
Multiplicative systematic uncertainties (%)						
Tracking	2.0	2.0	1.0	1.0	1.5	1.5
PID	2.0	2.0	1.0	1.0	1.5	1.5
π^0 reconstruction	2.0	2.0	6.0	6.0	4.0	4.0
ΔE requirement	1.7	1.7	1.7	1.7	0.3	0.3
K_S^0 veto	0.8	0.8	1.4	1.4	0.8	0.8
ω/η signal region	0.2	0.2	0.2	0.2	0.2	0.2
MC generator	2.0	3.0	$(\cdots)$	$(\cdots)$	3.5	3.5
ST yield	1.2	1.2	1.2	1.2	0.4	0.4
Strong phase in D^0 decays	7.3	0.8	7.3	7.3	$(\cdots)$	$\cdots$
$\mathcal{B}(\omega/\eta \to \pi^+\pi^-\pi^0)$	0.8	1.2	0.8	1.2	0.8	1.2
$\mathcal{B}(\pi^0 \to \gamma\gamma)$	Negl.	Negl.	Negl.	Negl.	Negl.	Negl.
Total	8.7	5.3	9.9	10.0	5.9	6.0

VI. RESULTS

The absolute BFs of $D^0 \to \omega/\eta\pi^+\pi^-$ and $D^+ \to \omega/\eta\pi^+\pi^0$ are calculated with Eq. (1). Since the significance of $D^0 \to \omega/\eta\pi^0\pi^0$ is less than 1σ, we compute upper limits on the BFs for these two decays at the 90% confidence level (C.L.) by integrating their likelihood versus BF curves from zero to 90% of the total curve. The effect of the systematic uncertainty is incorporated by convolving the likelihood curve with a Gaussian function with a width equal to the systematic uncertainty. All results are summarized in Table III.

VII. SUMMARY

In summary, we perform the BF measurements of SCS decays $D \to \omega\pi\pi$ using 2.93 fb^{-1} of $\psi(3770)$ data sample collected by the BESIII detector. The BFs of $D^0 \to \omega\pi^+\pi^-$ and $D^+ \to \omega\pi^+\pi^0$ are determined to be $(1.33 \pm 0.16 \pm 0.12) \times 10^{-3}$ and $(3.87 \pm 0.83 \pm 0.25) \times 10^{-3}$, respectively. The precision of the BF for $D^0 \to \omega\pi^+\pi^-$ is improved by a factor 2.1 over the CLEO measurement [6] and the decay process $D^+ \to \omega\pi^+\pi^0$ is measured for the first time. These measurements are important inputs to beauty physics to improve the precision of the CKM angle γ via $B^\pm \to D^0(\to \omega\pi^+\pi^-)K^\pm$ [1,3] and the semitauonic decay $B^0 \to D^{*\pm}\tau^\mp(\to \pi^+\pi^-\pi^\mp)\nu_\tau$ [4]. No evidence of $D^0 \to \omega\pi^0\pi^0$ is found, and the upper limit on the BF at the 90% C.L. is 1.10×10^{-3}. Meanwhile, the BFs of $D^0 \to \eta\pi^+\pi^-$ and $D^+ \to \eta\pi^+\pi^0$ as well as the upper limit on the BF of $D^0 \to \eta\pi^0\pi^0$ at 90% C.L. are measured to be $(1.06 \pm 0.18 \pm 0.07) \times 10^{-3}$, $(2.47 \pm 0.93 \pm 0.16) \times 10^{-3}$, and less than 2.38×10^{-3}, respectively, with the decay mode $\eta \to \pi^+\pi^-\pi^0$. The results are consistent with previous measurements [25,27].

ACKNOWLEDGMENTS

The BESIII Collaboration thanks the staff of BEPCII, the IHEP computing center, and the supercomputing center of USTC for their strong support. This work is supported in part by National Key Basic Research Program of China under Contract No. 2015CB856700; National Natural Science Foundation of China (NSFC) under Contracts No. 11335008, No. 11375170, No. 11425524, No. 11475164, No. 11475169, No. 11605196, No. 11605198, No. 11625523, No. 11635010, No. 11705192, No. 11735014, No. 11822506, No. 11835012, No. 11935015, No. 11935016, No. 11935018, No. 11961141012, and No. 11950410506; 64th batch of Postdoctoral Science Fund Foundation under Contract No. 2018M642516; the Chinese Academy of Sciences (CAS) Large-Scale Scientific Facility Program; Joint Large-Scale Scientific Facility Funds of the NSFC and CAS under Contracts No. U1732263 and No. U1832207; CAS Key Research Program of Frontier Sciences under Contracts No. QYZDJ-SSW-SLH003 and No. QYZDJ-SSW-SLH040; 100 Talents

Program of CAS; INPAC and Shanghai Key Laboratory for Particle Physics and Cosmology; ERC under Contract No. 758462; German Research Foundation DFG under Contracts No. Collaborative Research Center CRC 1044, No. FOR 2359; Istituto Nazionale di Fisica Nucleare, Italy; Ministry of Development of Turkey under Contract No. DPT2006K-120470; National Science and Technology fund; STFC (United Kingdom); Olle Engkvist Foundation under Contract No. 200-0605; The Knut and Alice Wallenberg Foundation (Sweden) under Contract No. 2016.0157; The Royal Society, UK under Contracts No. DH140054 and No. DH160214; The Swedish Research Council; U.S. Department of Energy under Contracts No. DE-FG02-05ER41374 and No. DE-SC-0012069.

[1] M. Gronau and D. London, Phys. Lett. B **253**, 483 (1991); M. Gronau and D. Wyler, Phys. Lett. B **265**, 172 (1991).
[2] D. Atwood, I. Dunietz, and A. Soni, Phys. Rev. D **63**, 036005 (2001); Phys. Rev. Lett. **78**, 3257 (1997).
[3] A. Giri, Y. Grossman, A, Soffer, and J. Zupan, Phys. Rev. D **68**, 054018 (2003); A. Bondar, in *Proceedings of the BINP Special Analysis Meeting on Dalitz Analysis, September 24–26, 2002* (unpublished).
[4] Heavy Flavor Averaging Group (HFLAV), http://www.slac.stanford.edu/xorg/hflav/charm/.
[5] G. Caria *et al.* (Belle Collaboration), Phys. Rev. Lett. **124**, 161803 (2020).
[6] P. Rubin *et al.* (CLEO Collaboration), Phys. Rev. Lett. **96**, 081802 (2006).
[7] M. Ablikim *et al.* (BESIII Collaboration), Chin. Phys. C **37**, 123001 (2013); Phys. Lett. B **753**, 629 (2016).
[8] R. M. Baltrusaitis *et al.* (MARK-III Collaboration), Phys. Rev. Lett. **56**, 2140 (1986); J. Adler *et al.* (MARK-III Collaboration), Phys. Rev. Lett. **60**, 89 (1988).
[9] M. Peshkin and J. L. Rosner, Nucl. Phys. **B122**, 144 (1977).
[10] M. Gronau and J. L. Rosner, Phys. Rev. D **79**, 074022 (2009).
[11] M. Ablikim *et al.* (BESIII Collaboration), Nucl. Instrum. Methods Phys. Res., Sect. A **614**, 345 (2010).
[12] S. Agostinelli *et al.* (GEANT Collaboration), Nucl. Instrum. Methods Phys. Res., Sect. A **506**, 250 (2003).
[13] S. Jadach, B. F. L. Ward, and Z. Was, Phys. Rev. D **63**, 113009 (2001).
[14] M. Tanabashi *et al.* (Particle Data Group), Phys. Rev. D **98**, 030001 (2018) and (2019) update.
[15] D. J. Lange, Nucl. Instrum. Methods Phys. Res., Sect. A **462**, 152 (2001); R. G. Ping, Chin. Phys. C **32**, 599 (2008).
[16] J. C. Chen, G. S. Huang, X. R. Qi, D. H. Zhang, and Y. S. Zhu, Phys. Rev. D **62**, 034003 (2000).
[17] H. Albrecht *et al.* (ARGUS Collaboration), Phys. Lett. B **241**, 278 (1990).
[18] J. E. Gaiser, Ph. D. thesis [Report No. SLAC-R-255, 1982 (unpublished)]; M. J. Oreglia, Ph. D. thesis [Report No. SLAC-R-236, 1980 (unpublished)]; T. Skwarnicki, Ph.D. Thesis [Report No. DESY-F-31-86-02, 1986 (unpublished)], https://en.wikipedia.org/wiki/Crystal_Ball_function.
[19] M. Ablikim *et al.* (BESIII Collaboration), Phys. Rev. D **98**, 032001 (2018).
[20] M. Ablikim *et al.* (BESIII Collaboration), Phys. Rev. D **97**, 072004 (2018).
[21] M. Ablikim *et al.* (BESIII Collaboration), Eur. Phys. J. C **76**, 369 (2016).
[22] K. S. Cranmer, Comput. Phys. Commun. **136**, 198 (2001).
[23] T. Gershon, J. Libby, and G. Wilkinson, Phys. Lett. B **750**, 338 (2015).
[24] T. Evans, S. T. Harnew, J. Libby, S. Malde, J. Rademacker, and G. Wilkinson, Phys. Lett. B **757**, 520 (2016).
[25] M. Ablikim *et al.* (BESIII Collaboration), Phys. Rev. D **101**, 052009 (2020).
[26] M. Ablikim *et al.* (BESIII Collaboration), Chin. Phys. C **44**, 040001 (2020).
[27] M. Ablikim *et al.* (BESIII Collaboration), Phys. Lett. B **781**, 368 (2018).